16. Development of birefringence free ridge waveguides for waveguide isolators

Sponsor:
DARPA

Project staff:
Xiaoyun Guo, Tauhid Zaman, Professor Rajeev Ram, Professor Henry I. Smith

Waveguide isolators that can be easily integrated with other components are essential to large scale photonic integration. Not only do these components provide functionality that cannot be achieved in integrated circuits today, but they also enable complex circuit design by isolating or 'buffering' the various parts of a circuit. This project is to develop a waveguide isolator on InP.

The central part of the isolator –Faraday rotator – can be fabricated from Fe:InP and Fe:InGaAsP. Magnetic dopants couple to the free carriers in a semiconductor to dramatically enhance the Faraday rotation due to interband transitions. With an appropriate choice of magnetic dopant, the free-carrier concentration can be reduced along with free-carrier absorption. In this way it is possible to *simultaneously* enhance the magneto-optical activity and reduce the optical absorption of a semiconductor.

Fe-doped InP with an Fe concentration of 2.9 x 10^{16} cm^{-3} was measured. At 1550 nm, the Verdet coefficient is 23.8 °/cm/T and the absorption coefficient is 0.20 cm^{-1}. Figure 1 shows the optical insertion loss encountered for 45° rotation through this material; an insertion loss of less than 2 dB is maintained over the entire wavelength range. The loss obtained for a 45° rotation at 1550 nm at 1 T is 1.66 dB, whereas with the previous estimates it was close to 172 dB.

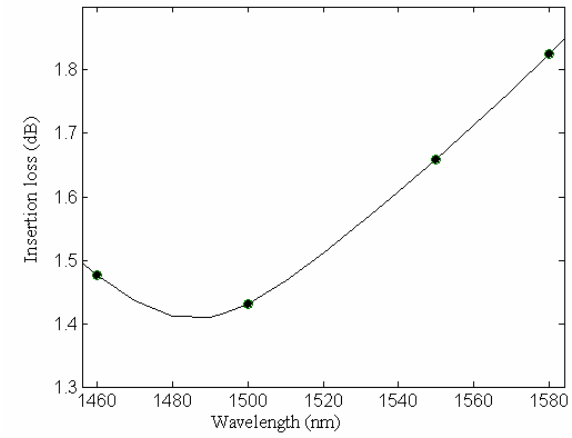

***Figure 1**. Optical insertion loss obtained for a 45° rotation in magnetically doped InP under a 1 T magnetic field vs. optical wavelength. The absorption coefficient and Verdet coefficient are all measured values in InP with an Fe concentration of 3x10^{16} cm^{-3}.*

Incorporation of magnetically doped semiconductors into optical devices, either in resonator or waveguide geometries, is also explored. A vertical cavity Fabry-Perot resonator was fabricated with 303 μm cavity length, consisting of highly doped InP/InGaAsP/InP at 1μm:0.53μm:1.5μm (Fe concentration of 1x10^{17} cm^{-3}) grown on a weakly doped InP substrate (Fe concentration of 1x10^{16} cm^{-3}). Faraday rotation was measured on resonance and off resonance. Reversal of the magnetic field confirms that the rotation is non-reciprocal.

17. Nanomagnets and Magnetic-random-access memories

Sponsors:
Cambridge-MIT Institute, National Science Foundation

Project Staff:
Fernando J. Castaño, W. Jung Prof. Caroline A. Ross and Prof. Henry I. Smith
in collaboration with J. A. C. Bland, Cambridge University

We are using a variety of lithography techniques (electron-beam lithography, interference lithography, zone-plate-array lithography, photolithography and X-ray lithography) to fabricate devices based on arrays of pillars, bar-shaped, and ring-shaped 'nanomagnets'. These tiny structures have thicknesses of a few nanometers and lateral dimensions typically smaller than 100 nm. Arrays of these elements are made with spatial periods of 100 nm and above, using evaporation/sputtering and liftoff, or by etching of a sputtered film. We are exploring the switching mechanisms of these particles, the thermal stability of their magnetization, and interparticle interactions, and we are assessing their suitability for various data-storage schemes. The behavior of individual particles can be measured using magnetic-force microscopy (MFM), while the collective behavior of arrays of particles can be measured using magnetometry. Comparison of these data shows how the behavior of one magnet is affected by its neighbors, and how much intrinsic variability there is between the particles as a result of microstructural differences. Small particles have near-uniform magnetization states, while larger ones develop more complex structures such as magnetization vortices or domain walls.

These nanomagnets have potential uses in magnetic-random-access memories (MRAM), magnetic logic devices and other magneto-electronic applications. Current MRAM devices rely on bar-shaped multilayered nanomagnets, containing two magnetic layers separated by a thin layer of either a non-magnetic metal (Spin-valves) or an isolator (Magnetic tunneling junctions). The resistance of such elements depends on the relative orientation between the magnetization in the read-out (free) and storage (pinned) layers, allowing for a non-volatile bit of data to be stored in each element. An alternative possibility for high-density MRAMs is to use ring-shaped nanomagnets, in which a bit of information could be stored by magnetizing the ring clockwise or counterclockwise. Micron-sized rings had been shown to display two different magnetic states: one being the flux-closure or 'vortex' state (with clockwise or counter-clockwise magnetization) and the other a state with two domain walls, known as an 'onion' state.

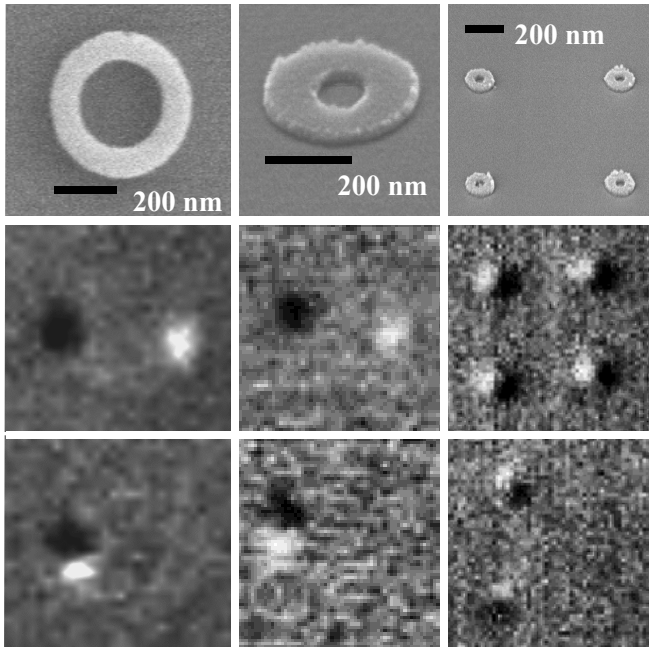

Figure 1. Top row: Scanning electron micrographs (SEM) of Co rings with outer diameters of 500 nm (left), 360 nm (middle) and 180 nm (right column). The larger ring is shown in plan view while the other rings are shown tilted. Middle row: MFM remanent images after saturating the sample in a field of 10 kOe, showing onion states. Bottom row: MFM scans after applying reversing fields of 216 Oe, 1000 Oe, and 1700 Oe, respectively. The images show twisted states, except for two of the smallest rings which are in the vortex state and therefore show no contrast.

Unexpectedly, we found that magnetic rings with submicron diameters display new metastable states, called twisted states, consisting of a vortex state containing a 360˚ wall. The existence of twisted states in nanorings has interesting consequences for the design of magnetoelectronic devices.

For applications where it is desirable to pin the walls in certain places, we have shown that control over the position of the domain walls can be achieved by distorting the ring into an ellipse. The anisotropic behavior of elliptical rings, in particular the difference in stability range of the vortex states as a function of the applied field direction, provide additional control over the switching behavior and may be useful in MRAM or other magnetoelectronic devices where it is desirable to reproducibly create and move domain walls.

Most recently we are fabricating MRAM prototypes based on circular and elliptical ring nanomagnets. The rings in these devices consist in multilayered structures such as spin valves and magnetic tunneling junctions. The fabrication process starts with a photo-lithographically defined contact chip. The ring structure and the final contacts are defined by e-beam lithography and lift off processing. For these devices to be operative the alignment accuracy for the final contacts of the ring has to be within a few tens of nanometers. Each magnetic memory chip contains up to 15 devices which are connected between them, allowing for both reading and writing processes to be undertaken.

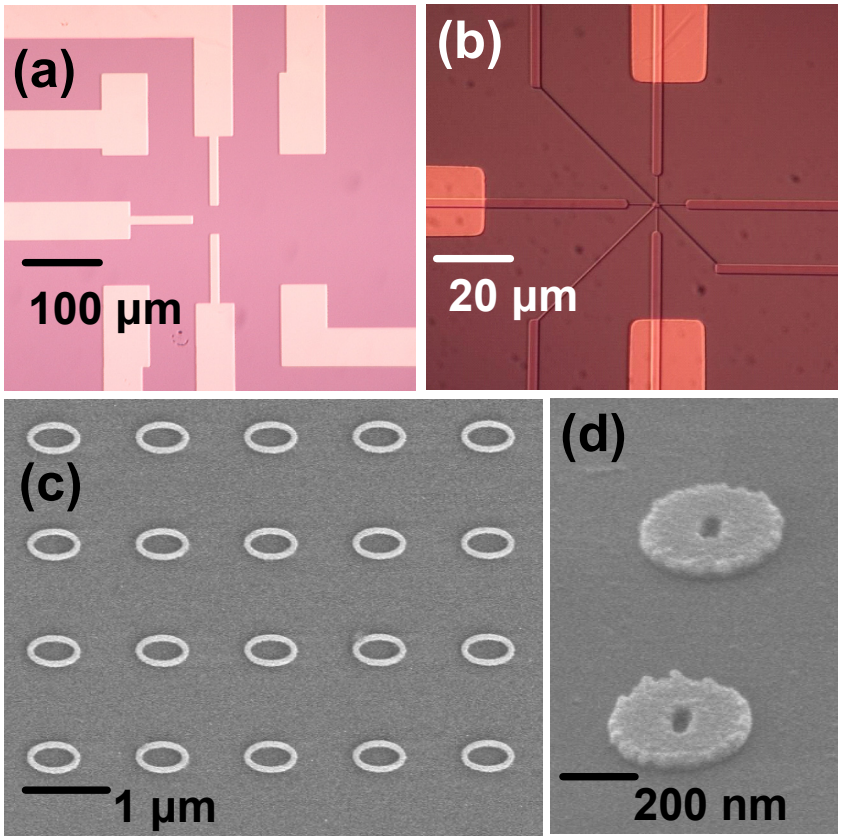

Figure 2. **(a)** Optical micrograph corresponding to one of the contact devices in a prototype ring-MRAM chip. **(b)** Micrograph showing the final contact patterns to a ring, written in a 450K PMMA (150 nm)/ 950K PMMA (120 nm) resist structure. **(c)** SEM micrographs of arrays of multilayered elliptical rings containing a multilayer stack of NiFe (6 nm)/Cu (4 nm)/ Co (4 nm) **(d)** Rings containing multilayer stack of NiFe (6 nm)/ $Al_2 O_3$ (7 Å)/ CoFe (4 nm).

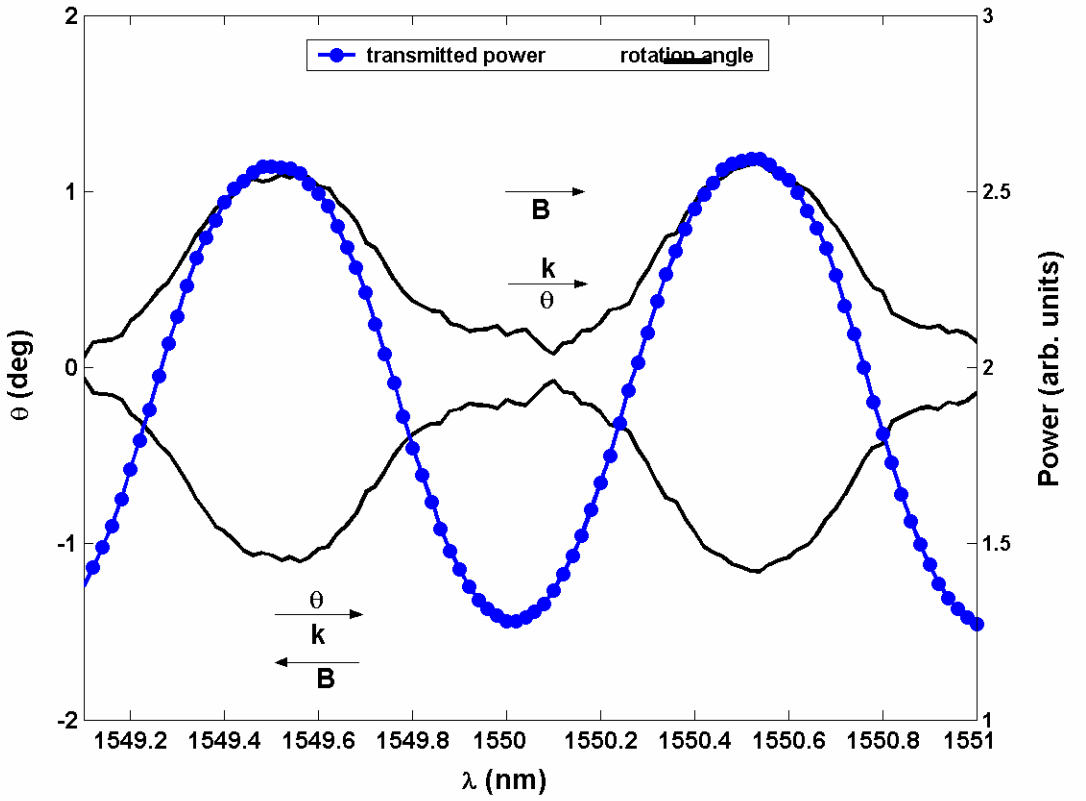

***Figure 2**. The smooth lines indicate the rotation angle for linear polarization upon transmission through InP/InGaAsP/InP resonator with a Fe concentration of 1x10^{17} cm^{-3}, grown on a 300 μm InP substrate with an Fe concentration of 1x10^{16} cm^{-3}. The magnetic field is 0.5T. The direction of the B field for upper line and lower line is as shown. For reference, the power transmission spectrum is also shown as the linen with dot markers.*

Realization of integrated Faraday rotators requires that magneto-optical materials be incorporated in a waveguide where TE and TM modes have nearly equal propagation constants. High-index-contrast waveguides are designed and fabricated to achieve zero birefringence. The waveguides consist of an InGaAsP core layer and Fe-doped InP cladding layers. To achieve appreciable Faraday rotation for the Verdet coefficients measured above, the difference of propagation constants between TE and TM modes must be less than 10^{-5}. The waveguide width versus wavelength for zero birefringence is shown in Fig.3 when the etching depth is 2.5μm. The inset shows the experimental realization of this waveguide design. Preliminary measurements on magnetically doped waveguides confirm that $\Delta\beta<10^{-3}$.

Processing was developed to fabricate waveguides for zero birefringence and lowest propagation loss. This device will be integrated directly with other device such as semiconductor optical amplifiers in the future.

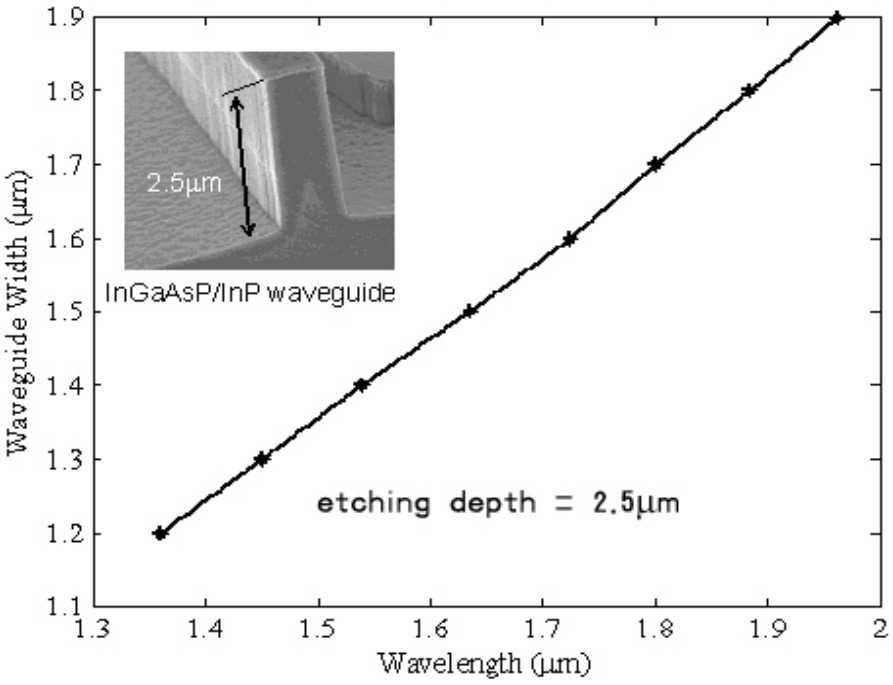

***Figure** 3. Waveguide width vs wavelength to achieve zero birefringence.*

In summary, these measurements show that InP based integrated Faraday rotators with low insertion loss can be achieved.

19. Fabrication and Assembly of Metallic Nano-Wires, Rods, and Dots for Micro- and Nano-Systems (MAT)

Sponsors:
NSF, MARCO

Project Staff:
Amanda L. Giermann, Ramkumar Krishnan, R. Tadepalli, and Professor Carl V. Thompson

Collaborators:
Dr. Fernando Castano, W.K. Choi, Professor Eugene A. Fitzgerald, N.Q. Hung, Kornelius F. Nielsch, N. Quitoriano, Professor Caroline A. Ross, Professor Francesco Stellacci, , Professor Henry I. Smith

Metallic nano-wires, rods, and dots can be used in a number of applications in micro- and nano-systems, such as nanowire-interconnects (wires), on-chip magnetic storage devices (rods), on-chip Peltier cooling devices (wires and rods), and plasmonic waveguides (dots). We are developing new methods that combine top-down (lithography) and bottom-up (self-assembly) approaches for fabricating and assembling metallic nano-wires, rods, and dots, for new applications including nano-contacts for devices and interconnects for mixed-material and multifunctional micro- and nano-systems.

Anodic porous alumina is an example of a self-ordered nano-structured material that is well-suited as a template for growing metallic and semiconductor nanostructures. When aluminum is anodized, the resulting oxide film contains an arrangement of pores or channels running vertically through the film. The pores form a structure with local hexagonal order, but lack any long range order. We have developed a technique to obtain single-domain porous alumina on silicon with controlled pore-spacing and diameter in hexagonal as well as square arrays (Fig. 1, 2). This is done by etching an array of shallow holes into a silicon wafer, coating the wafer with an aluminum film, and then anodizing the film to form alumina. The pores in the alumina film form in places determined by the pattern originally etched into the silicon. Additionally, by changing the anodization conditions, we have achieved ordering of pores on a sub-lithographic length scale. Using this template-assisted self-assembly technique, we have fabricated metallic nanodots (Fig. 3), nanorods (Fig. 4), nanotubes (Fig. 5) and antidot structures (films with regular hole patterns) all of which have properties very different from their bulk counterparts. We are also studying the effect of chemical and electrochemical processing conditions on the microstructure and material properties of nanowires and nanotubes. We are currently exploring the use of metal-filled alumina templates as *electrical nano-breadboards* for molecular electronics applications using techniques such as dip-pen nanolithography. Other areas of current work include catalyst-assisted growth of ordered semiconductor nanowires and carbon nanotubes in porous alumina templates.

We are also investigating templated self-assembly (TSA) as a route to fabrication of ordered arrays of nano-dots and nano-wires. Templated self-assembly is a self assembly process on a surface patterned with conventional lithography techniques that leads to long-range periodic structures with a final characteristic length scale that is smaller than that of the initial pattern, thus overcoming the minimum size limitations of standard lithography. Our approach is to create ordered metallic nano-particles by annealing thin films at high temperatures. When a polycrystalline film is annealed at high temperatures, the grain boundaries form grooves at the surface. These grooves deepen to intercept the film/substrate interface. Once such voids form, the film proceeds to agglomerate into individual islands, resulting in a field of micro- or nano-particles. In earlier studies, we have characterized this process in films deposited on planar surfaces. We are developing methods to induce these islands to self-align by agglomerating them on various lithographically defined periodic topographies.

Ordered arrays of metallic nano-particles play an important role as catalysts for semiconductor nano-wire growth by the metal-mediated vapor-liquid-solid CVD technique. The material system is chosen such that the metal catalyst and the semiconductor form a deep eutectic, allowing for liquid droplet formation at relatively low temperatures. The CVD precursors preferentially deposit on the metallic catalysts, forming a liquid droplet above the eutectic temperature. As deposition continues, the droplets become supersaturated and semiconductor material is precipitated at the droplet-substrate
interface, forming a semiconductor nano-wire. We have successfully grown GaAs nano-wires via this technique using randomly distributed gold nano-particles as catalysts and we are working to understand and control the growth process as well as explore TSA as a technique to grow ordered array of semiconductor nanowires.

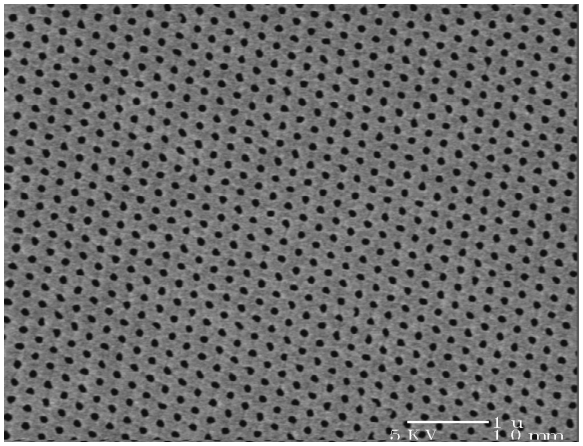

Figure 1 *Hexagonal array ordered porous alumina on Si. Pores were formed by anodizing evaporated aluminum on silicon containing a hexagonal array of indentations in 5% H_3PO_4 at 86V (Pore dia = 80nm, spacing = 200nm).*

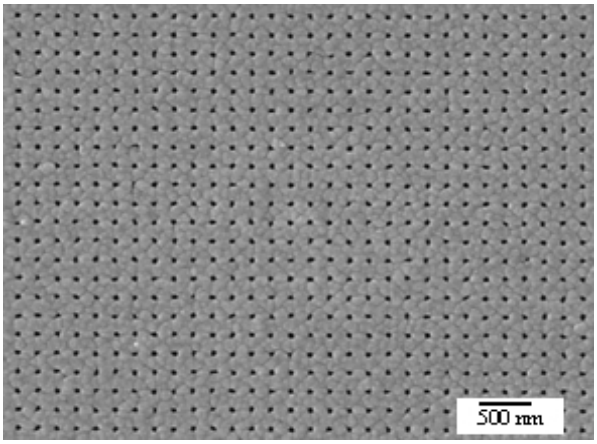

Figure 2 *Square lattice of pores of 30nm diameter formed by anodizing at 89V using 0.1M oxalic acid.*

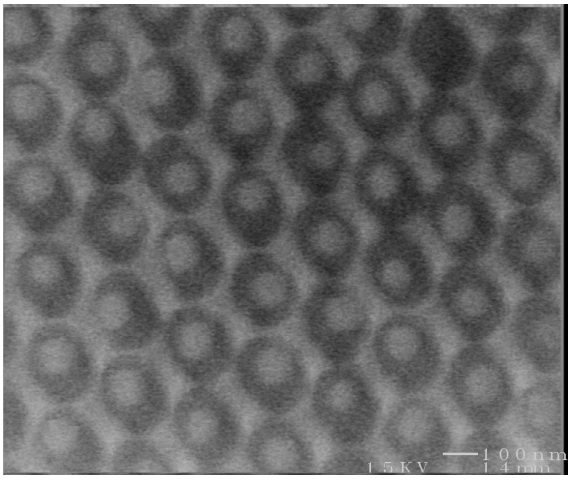

Figure *3. Nickel nanodots deposited by evaporation using ordered alumina template as mask.*

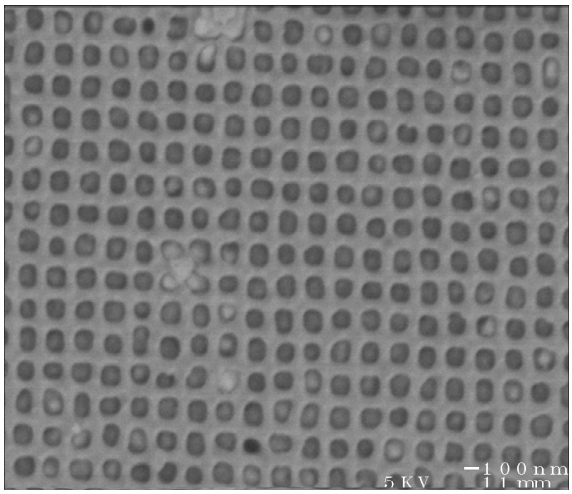

Figure *4. Copper nanorods electrodeposited using ordered porous alumina on Silicon. Variations in contrast of nanorods due to variation in fill rate. Aluminum in Ti/Au/Al multilayer stack was anodized to reach the gold underlayer and copper was electrodeposited on gold using acid sulfate solution.*

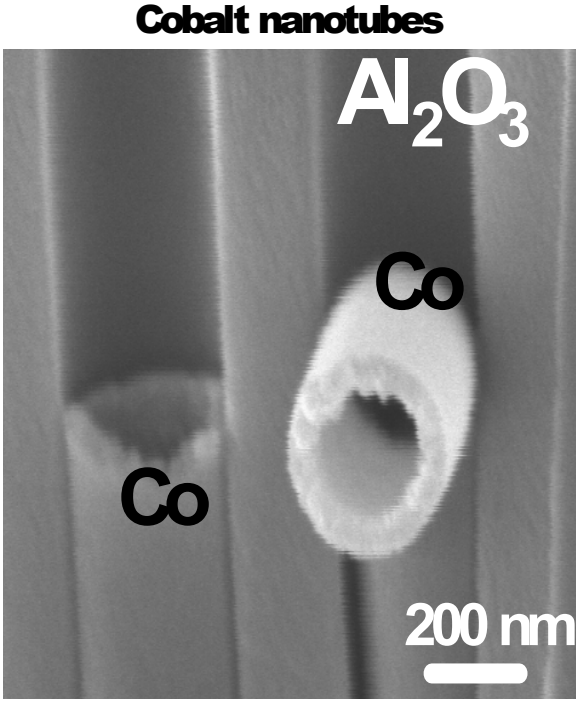

***Figure** 5. Cobalt nanotubes in Porous alumina. Formed by reduction of cobalt carobonyl salt dissolved in PLLA/Dichloromethane solution at 180C. PLLA was removed thereafter by thermal decomposition at 300C.*

20. Measuring the Thermal Properties of Nanowires

Sponsors:
DOE BES (DE-FG02-02ER45977) and NSF (CTS-0129088).

Project Staff:
Chris Dames, Mark Mondol, Prof. Gang Chen, and Prof. Henry I. Smith.

Nanowires are an important building block for nanotechnology, with potential applications in computing, optoelectronics, molecular sensing, and thermoelectrics. It is known that the thermal properties of nanowires may differ from the bulk because of both classical and quantum size effects. The primary goal of this project is to fabricate test structures to measure the specific heat of nanowires as a function of diameter and temperature. This will not only elucidate the basic scientific question of the dimensionality of phonons in nanowires, but may also be used as platform for extraordinarily sensitive calorimetry.

Two complementary approaches are outlined below: (1) a single-nanowire 4-point probe fabricated with electron-beam lithography; and (2) a "bulk" measurement of large arrays of uniform-diameter nanowires grown from catalysts patterned by interference lithography. The nanowires to be used initially are ZnO, 50-100 nm diameter, and 3-5 um long (provided by Debasish Banerjee and Prof. Zhifeng Ren, Dept. of Physics, Boston College).

(1a) Scanning electron-beam lithography for single nanowire test structures.

The first step in fabrication (Fig. 1) is to use contact lithography and lift-off to pattern a gold fiducial grid on top of the device layer of an SOI wafer. Then ZnO nanowires are spread randomly over the substrate, either by lightly grinding a powder of nanowires, or by dispersing and drying out a nanowire suspension. Optical and scanning electron microscopy are then used to find straight, clean, isolated nanowires, and record their locations with respect to the fiducial grid. Based on the locations of these candidate nanowires, a unique mask file is generated using the recently-developed MATKIC scripts (described further below). The mask file is used with the VS-26 e-beam lithography tool to pattern PMMA for another gold lift off step, forming the 4-point probes and bond pads. Finally, a KOH or TMAH wet etch is used to remove part of the SOI device layer, so that the nanowire is suspended above the substrate for thermal isolation.

Scanning electron-beam lithography is used because of its very high spatial resolution, and because it is maskless, which facilitates rapid turnaround. Initially troublesome field-stitching errors have been resolved by combining a global map of the coordinate systems with a one-time alignment of the field to known points on the gold fiducial grid, reducing the errors by at least an order of magnitude.

(1b) "MATKIC" scripts for rapid parametric design of KIC mask files.

The KIC file for each set of nanowire bond pads may require hundreds or even thousands of individual "Manhattan-geometry" boxes. Rather than drawing each box manually in standard KIC software such as NanoWriter or x-kic, a collection of MATLAB scripts has been developed to easily create arbitrary mathematical shapes in the KIC format. MATKIC may prove useful to anyone using KIC or CIF format mask files for arrays and/or non-Manhattan geometries. Figure 2 gives one example of the kinds of parametric variations that are easily specified with just a few lines in MATKIC. Further information may be found at http://web.mit.edu/cdames/www/matkic/.

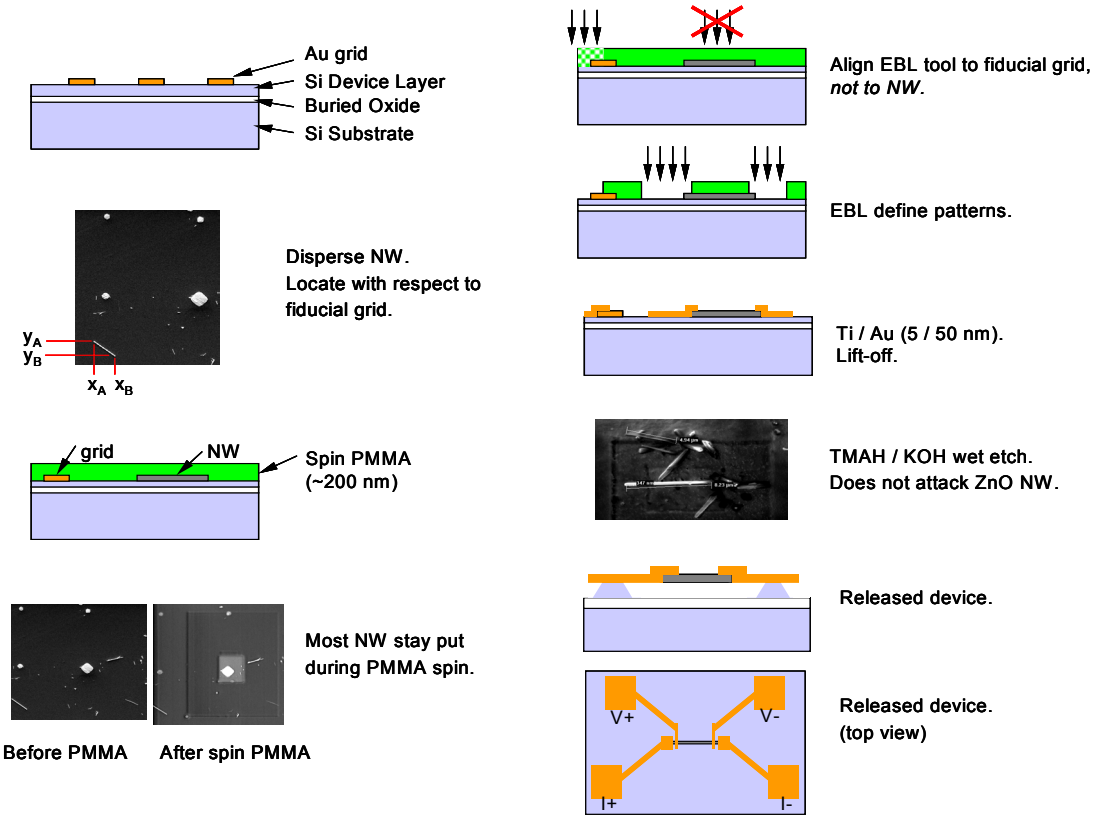

Figure 1. *Process flow for 4-point nanowire probes by e-beam lithography.*

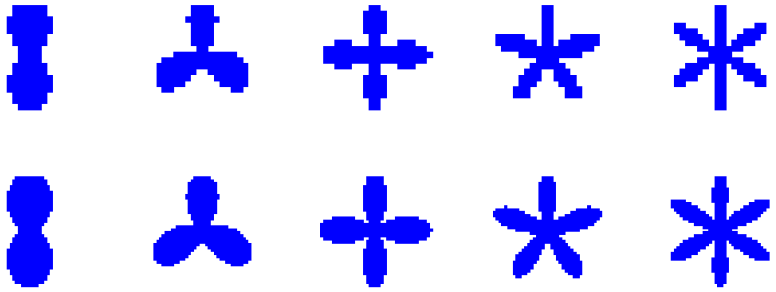

Figure 2. *Example of a parametric study of KIC shapes made with MATKIC.*

(2) Lloyd's mirror interference lithography for arrays of uniform nanowires.

Interference lithography will be used to create uniform arrays of gold or nickel dots on sapphire and/or silicon substrates. Because of the long-range spatial coherence intrinsic to interference lithography, these nanowire arrays are also expected to have interesting optical properties as 2-dimensional photonic crystals. They might also be useful for systematic studies of nanowire growth mechanisms.

The existing Lloyd's mirror interference lithography setup (λ=325 nm) will be used to create 2-dimensional square or hexagonal arrays using a tri-level resist stack and metal lift-off. To achieve the smallest possible nanowire diameters, the diameter of the metal dots should be minimized. Current work focuses on a systematic study of duty cycle as a function of dose at a nominal period of 180 nm.

21. Transmission Gratings for X-ray and Atom-Beam Spectroscopy and Interferometry

Sponsors:
X-OPT, Inc.

Project Staff:
James M. Carter, Timothy A. Savas, Professor Henry I. Smith and Dr. Mark L. Schattenburg

Transmission gratings with periods of 100 to 1000 nm are widely used in applications such as x-ray, vacuum-ultraviolet, and atom-beam spectroscopy and interferometry. Over 30 laboratories around the world depend on MIT-supplied gratings in their work. For x-ray and VUV spectroscopy, gratings are made of gold and have periods of 100 to 1000 nm, and thicknesses ranging from 100 to 1000 nm. The gratings are most commonly used for spectroscopy of the x-ray emission from high-temperature plasmas. Transmission gratings are supported on thin (1 micron) polyimide membranes, or made self supporting ("free standing") by the addition of crossing struts (mesh). (For short x-ray wavelengths, membrane support is desired, while for the long wavelengths, a mesh support is preferred in order to increase efficiency.) Fabrication is performed by interference lithography combined with reactive-ion etching and electroplating. Progress in this area tends to focus on improving the yield and flexibility of the fabrication procedures.

Another application is the diffraction of neutral-atom and molecular beams by mesh-supported gratings. Lithographic and etching procedures have been developed for fabricating free-standing gratings and grids in thin silicon-nitride (SiNx) membranes supported in a Si frame. Figure 1 shows a free-standing 100 nm-period grating in 100 nm-thick silicon nitride. Figure 2 shows a 100 nm-period grid in a 100 nm-thick SiNx membrane. Such a grid is used in experiments as a "molecular sieve."

We have established a collaboration with the Max-Planck Institute in Göttingen, Germany, in which they utilize our gratings of 100 nm period in diffraction experiments using atomic, molecular, and helium-cluster beams. As shown in Figure 3, the diffraction of atomic and molecular beams reveals striking deviations from Kirchhoff's optical diffraction theory. The analysis of the diffraction intensities enabled a quantitative determination of the attractive van der Waals interaction between the silicon nitride surface and various atomic and molecular species, including He, Ne, Ar, Kr, He*, Ne*, D_2, and CH_3F. The diffraction of cluster beams by a transmission grating has been established as a unique technique for the non-destructive mass selection and detection of small and weakly bound van der Waals clusters. Recently, the Göttingen group discovered bound states in mixed-isotope helium clusters, e.g. $^3He^4He_2$, $^3He^4He_3$, etc., by diffraction from one of our 100-nm-period gratings as shown in Figure 4. They also employed the grating to measure the bond length of the helium dimer, $^4He_2$, which is assumed to be the weakest molecular bond. In addition, the high-resolving power of the transmission gratings have enabled the Göttingen group to discover the existence of magic numbers at N = 10, 11, 14, 22, 26, 27, and 44 atoms, as shown in Figure 5. Whereas magic numbers in nuclei and clusters are attributed to enhanced stabilities, this result is not expected for quantum fluid He clusters on the basis of numerous calculations.

Data obtained by helium-atom-beam diffraction at large incident angles showed Lyman ghosts in the spectrum. This data led to the development of new fabrication techniques to improve the quality of the free-standing gratings in silicon nitride. Diffraction spectra from gratings made with the improved process show no Lyman ghosts, illustrating the important synergy between applications and nanofabrication.

Successful diffraction experiments with beams of buckyballs (C60) have been carried out with our 100 nm-period, free-standing SiNx gratings by Dr. Markus Arndt of the University of Vienna. In

addition, our 100 nm-period, free-standing SiNx gratings can be lightly coated with metal. Prof. Herman Batelaan of the University of Nebraska-Lincoln has used such gratings in highly-successful diffraction experiments with beams of 500 eV electrons, as shown in Figure 6.

Our 100 nm-period free-standing SiNx gratings are also used for atom interferometry by two groups: those of Prof. Alexander Cronin of the University of Arizona and Prof. Bruce Doak of the State University of Arizona. Cronin's group interferes neutral beams of sodium atoms while Doak's group interferes helium beams (performed at the Max Planck Institute in Göttingen, Germany in collaboration with P. Toennies).

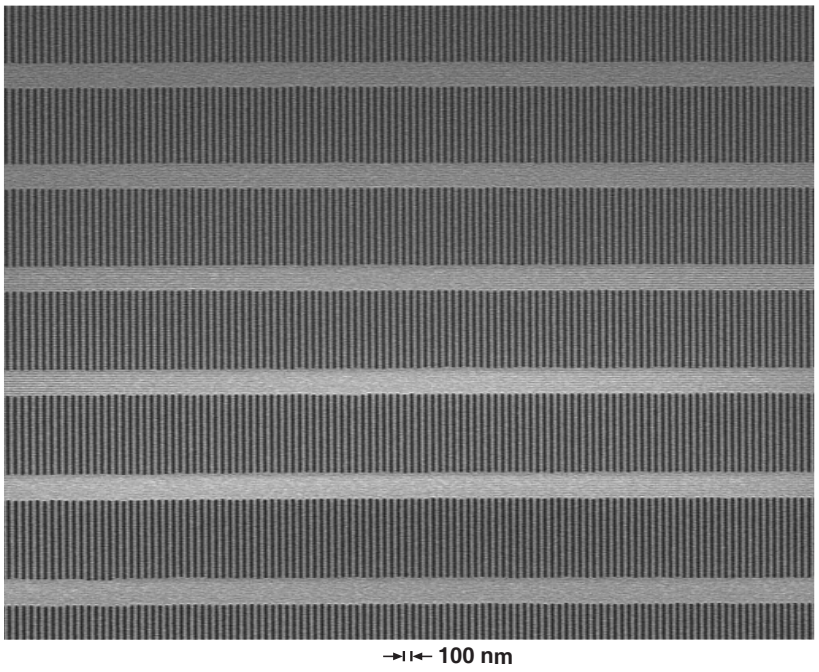

Figure 1. *Scanning electron micrograph of a free-standing 100 nm-period grating (50 nm-wide bars) in a silicon nitride membrane of area 500 microns by 5 mm.*

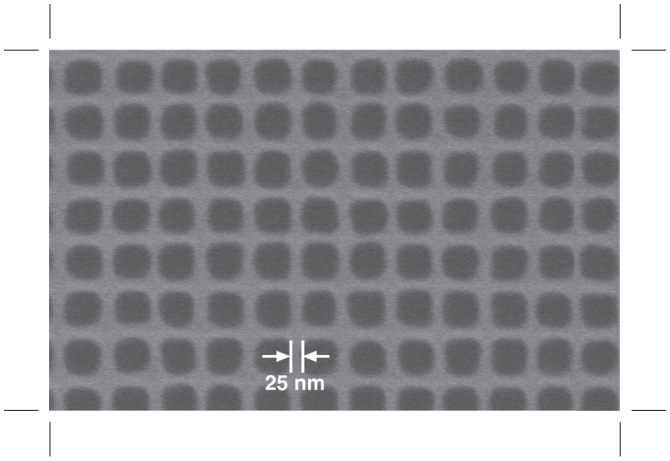

Figure 2. *Scanning electron micrograph of a free-standing 100 nm period grid in a silicon nitride membrane of area 500 micron by 5 mm. Such grids are used in experiments to separate out Helium trimers from other clusters.*

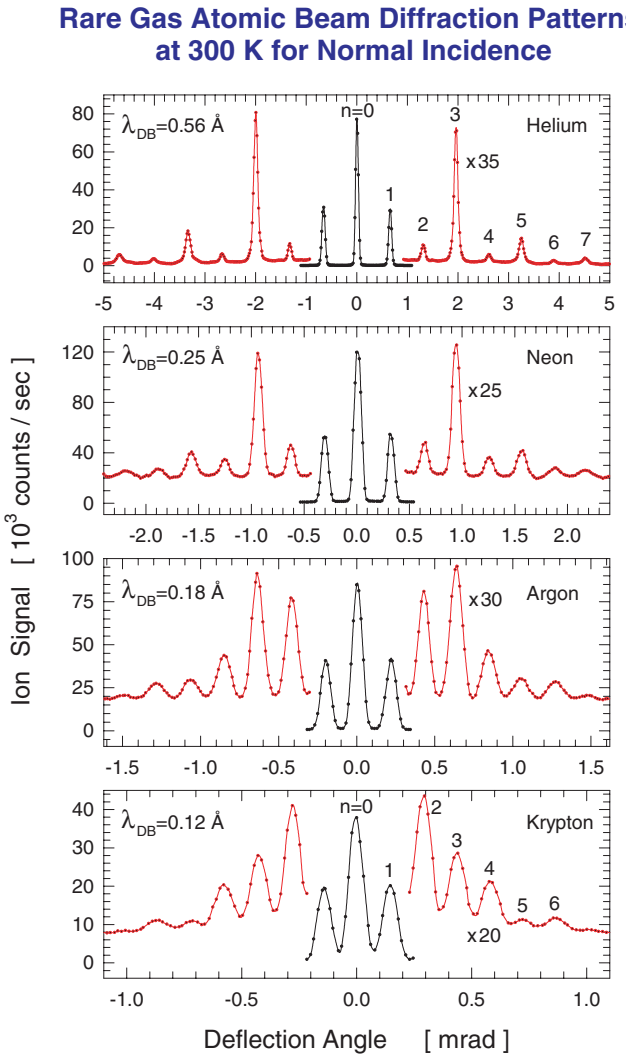

Figure 3. *Rare-gas atom-beam diffraction patterns. These results were obtained by Wieland Schöllkopf and Peter Toennies at the Max-Planck Institute in Göttingen, Germany, using a free-standing, 100nm-period grating*

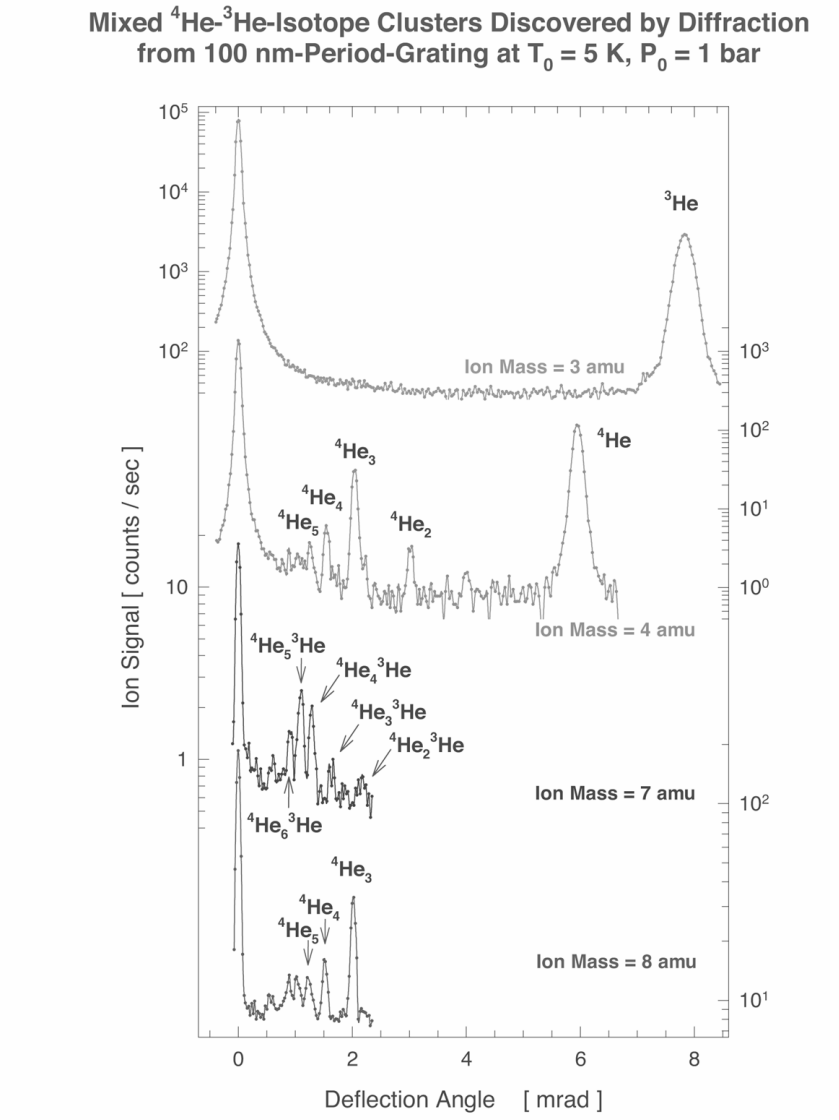

***Figure 4**. Non-destructive mass separation of small mixed-isotope helium clusters. These results were obtained by Peter Toennies, et al, at the Max-Planck Institute in Goettingen, Germany, using free-standing, 100 nm-period gratings made in the NSL at MIT.*

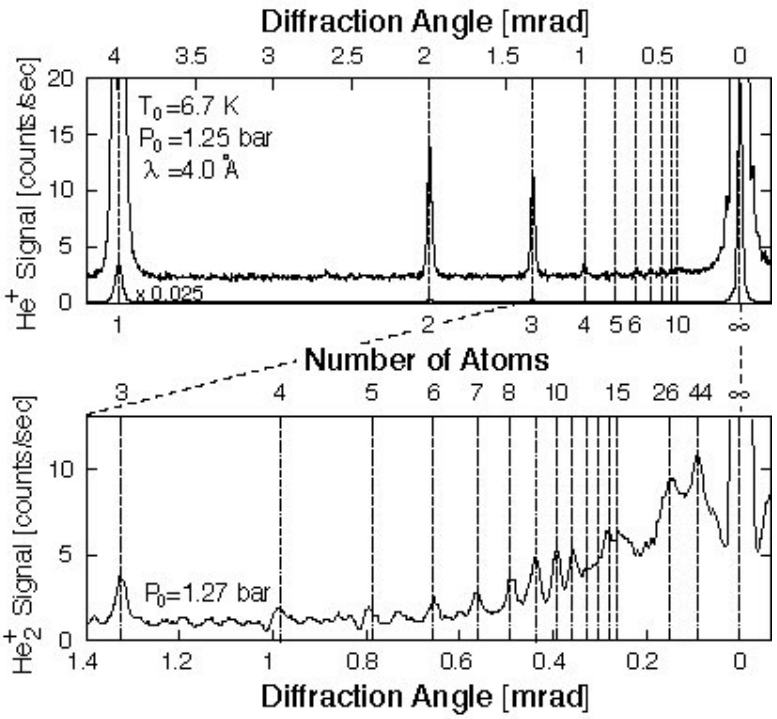

Figure 5. *Non-destructive mass separation of helium clusters that shows the existence of magic numbers. These results were obtained by Peter Toennies, et al, at the Max-Planck Institute in Goettingen, Germany, using free-standing, 100 nm-period gratings made in the NSL at MIT.*

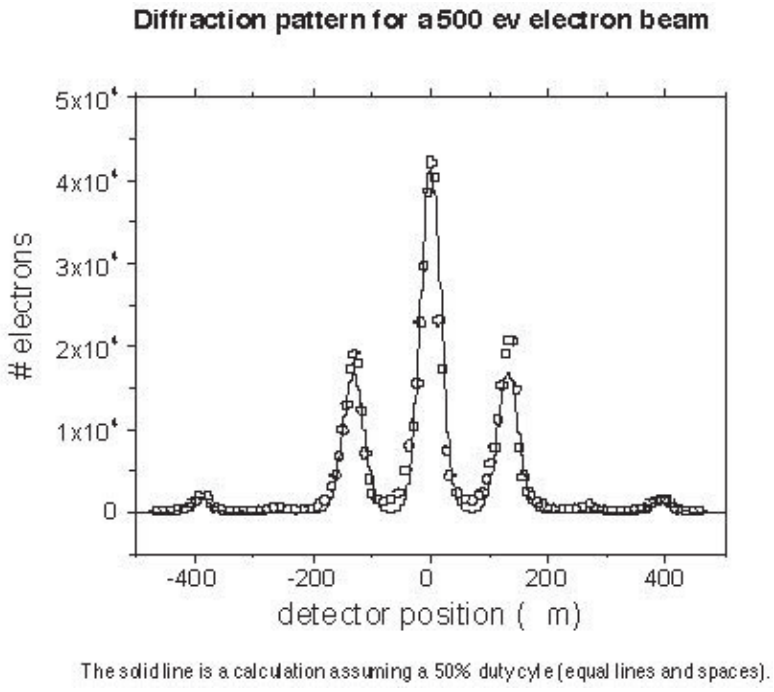

Figure 6. *Diffraction spectrum of 550 eV electrons. These results were obtained by Prof. Herman Batelaan of the University of Nebraska-Lincoln, using free-standing, 100 nm-period gratings made in the NSL at MIT.*

22. Nanofabricated Metal Transmission Gratings

Sponsors:
NASA (NAG5-5405) and XOPT, Inc.

Project Staff:
James Carter, Robert C. Fleming, Dr. Mark L. Schattenburg, Prof. Claude R. Canizares and Prof. Henry I. Smith

Wire-grid metal transmission gratings have many useful and novel optical properties that are enhanced when the grating period and/or slit dimensions approach or go below the wavelength of light. These benefits are particularly attractive in the UV and x-ray bands where the performance of conventional optics is poor. This benefit generally requires control of the grating period and feature dimensions in the nanometer to picometer range. In this research effort we are advancing metal transmission gratings past the already sophisticated technology developed at MIT over the past 20 years. Current research efforts seek to boost grating transmission efficiency, reduce defect levels, and improve control of grating feature geometry.

Our research group is the world leader in metal transmission grating fabrication technology and has used them in a wide variety of laboratory and space research applications. Over forty laboratories worldwide use MIT-fabricated transmission gratings for research, ranging from materials science to laser plasma fusion. Nine NASA missions have also utilized hundreds of MIT-fabricated transmission gratings in space research instruments ranging from x-ray spectrographs to atom imagers.

Metal transmission gratings are generally fabricated with electroplated gold and supported by submicron-thick polyimide membranes or coarse meshes of electroplated gold or nickel. The thin and fragile grating members require a carefully engineered coarse support mesh and metal frame to withstand the rigors of rocket launch and space environment. Transmission grating periods down to 100 nm and sizes up to 30x30 mm have been fabricated. Grating patterning is performed by interference lithography (IL) using a variety of novel tri-level resists schemes, followed by reactive-ion etching and metal electroplating. The combined resources of the MIT Nanostructures Lab (NSL) and Space Nanotechnology Lab (SNL) have been used to develop the most advanced IL tools in the world for high-yield fabrication of transmission gratings.

High-dispersion x-ray and extreme ultraviolet (EUV) transmission gratings were fabricated for NASA missions including the *Solar EUV Monitor* (SEM) on the *Solar and Heliospheric Observatory* (SOHO) mission, launched December 2, 1995, the *Chandra* x-ray telescope, launched July 23, 1999, and the *Geostationary Operational Environmental Satellites* (GOES N-Q) missions. The *Chandra* telescope provides high-resolution imaging and spectroscopy of x-ray-emitting astrophysical objects, with unprecedented power and clarity, which is significantly widening our view of the Universe. The SOHO and GOES satellite series perform solar EUV monitoring which provides early warning of solar flare events that could imperil satellite and astronaut operations.

A scanning-electron micrograph of a 200 nm-period gold grating from the *Chandra* mission is shown in Fig. 1. This grating is used in the High Energy Transmission Grating Spectrometer (HETGS) which provides high-resolution x-ray spectroscopy in the λ=0.1-14 nm band. Period control of 40 picometers was required to meet telescope resolution requirements. Figure 2 is an example of an x-ray spectra obtained by *Chandra* using our gratings.

Transmission grating filters were also fabricated for the *Medium Energy Neutral Atom* (MENA) instrument on the NASA *Magnetospheric Imaging Medium-Class Explorer* (IMAGE) mission,

launched March 25, 2000, and also for the NASA *Two Wide-Angle Imaging Neutral-atom Spectrometers* (TWINS A, B) Missions. Instruments on these missions provide neutral atom imaging of Earth's magnetosphere.

Transmission gratings are used to block the intense Hydrogen Lyman Alpha (λ=121.6 nm) deep-UV radiation that would otherwise overwhelm the sensitive atom detectors. Figure 2 depicts a 200 nm period atom nanofilter grating with 45 nm-wide slots, designed to block deep-UV radiation. Slot widths need to be controlled to within a few nanometers for optimal UV blocking.

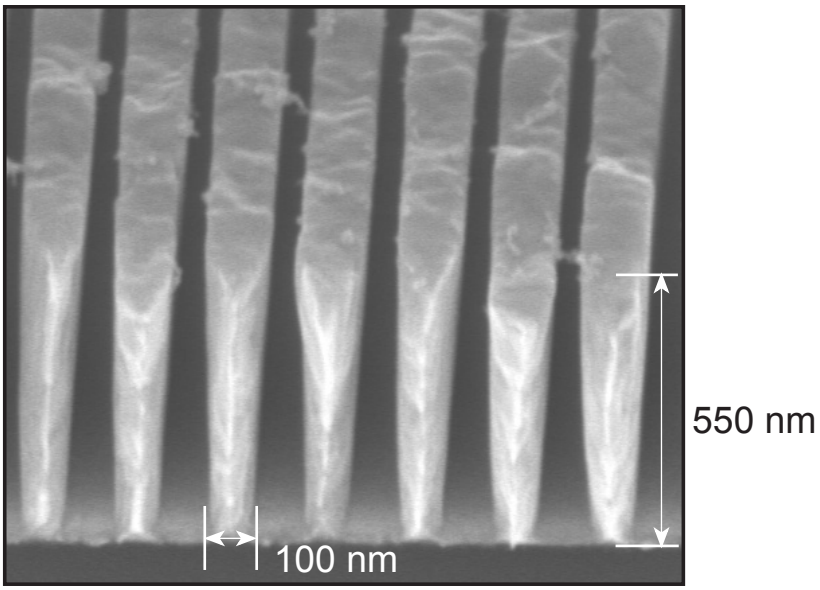

Figure 1 *Scanning-electron micrograph of a 200 nm-period gold x-ray transmission grating used in the HETGS instrument on the Chandra Observatory, cleaved to show the grating line sidewalls. The HETGS provides high-resolution x-ray spectroscopy in the λ=0.1-14 nm band. The gold bars are 100 nm wide, or approximately 400 gold atoms.*

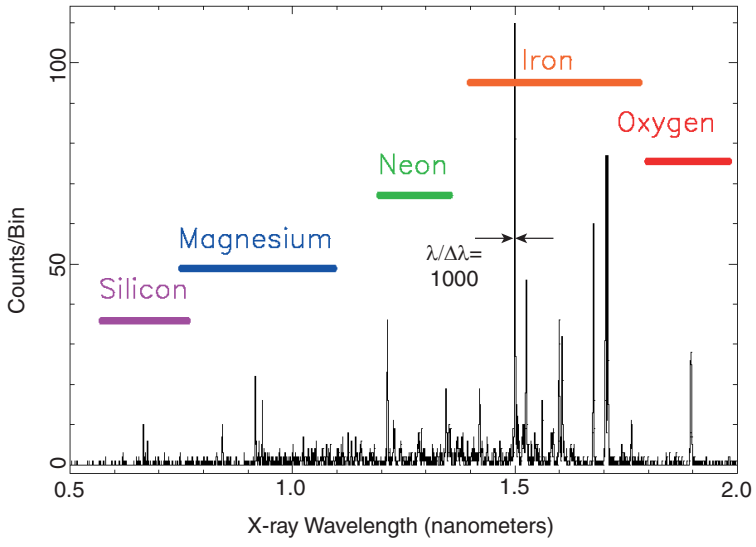

Figure 2 *X-ray spectra of the binary star Capella obtained via gold diffraction gratings on the* Chandra *x-ray astronomy satellite.*

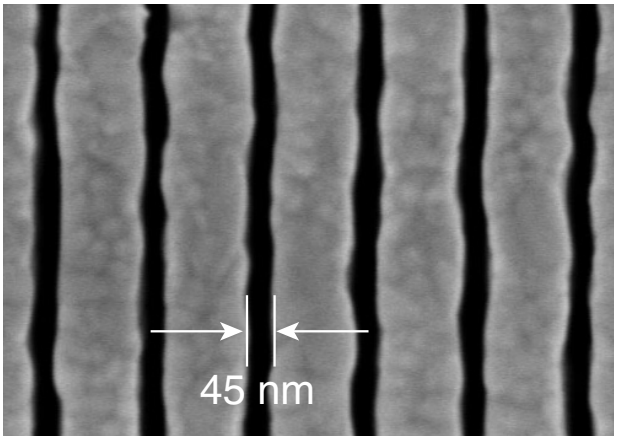

Figure 3. *Scanning-electron micrograph of a deep-UV blocking grating used in atom telescopes on the NASA IMAGE and TWINS missions. The grating blocks deep-UV radiation while passing energetic neutral atoms. Due to the narrow slot width of 45 nm and the large slot depth (~500 nm), the UV transmission is extremely low (~10−6 $\alpha\tau$ λ=121.6, while decreasing the transmitted atomic flux by only a factor of 10.*

23. Nanofabricated Reflection Gratings

Sponsors:
NASA (NAG5-5405, NAG5-12583), Chromaplex Corp., Nanonex Corp.

Project Staff:
James Carter, C.-H. Chang, Robert C. Fleming, Dr. Ralf Heilmann, Juan Montoya, Dr. Mark L. Schattenburg, Prof. Claude R. Canizares and Prof. Henry I. Smith

Grazing-incidence x-ray reflection gratings are an important component of advanced high-resolution spectrometers and other x-ray optics. These have traditionally been fabricated by diamond scribing with a ruling engine or by interference lithography followed by ion etching. These methods result in gratings which suffer from a number of deficiencies, including high surface roughness and poor groove profile control, leading to poor diffraction efficiency and large amounts of scattered light.

We are developing improved methods for fabricating blazed x-ray reflection gratings which utilize special (111) silicon wafers, cut 0.5-10 degrees off the (111) plane. Silicon anisotropic etching solutions, such as potassium hydroxide (KOH), etch the (111) planes very slow compared to other crystallographic directions, resulting in the desired super-smooth groove surface. Previous work used similar off-cut (111) silicon substrates to fabricate blazed diffraction gratings, but utilized a second KOH etch step that compromised the grating facet flatness and is unsuitable for small grazing-angle x-ray diffraction.

Gratings are patterned using interference lithography with the λ=351.1 nm wavelength, and transferred into substrates using tri-level resist processing, reactive-ion etching (RIE), and silicon-nitride masking during the KOH etch. The narrow (~100 nm) ridge of silicon which supports the nitride mask is removed using a novel chromium lift-off step followed by a CF_4 RIE. The result is extremely smooth sawtooth patterns, which, after applying a thin evaporative coating of Cr/Au, are suitable for x-ray reflection (see Fig. 1).

We are also developing UV and thermal nanoimprint lithography for low cost production of gratings. We have demonstrated the extremely high fidelity of the nanoimprint replication process, where added surface roughness is < 0.2 nm (see Fig. 2).

Potential applications of these improved gratings are for materials science research with synchrotron radiation and satellite-based high-resolution x-ray spectroscopy for planned NASA missions such as *Constellation X*. We are also exploring other applications for this technology, including telecom devices and atom microscopy.

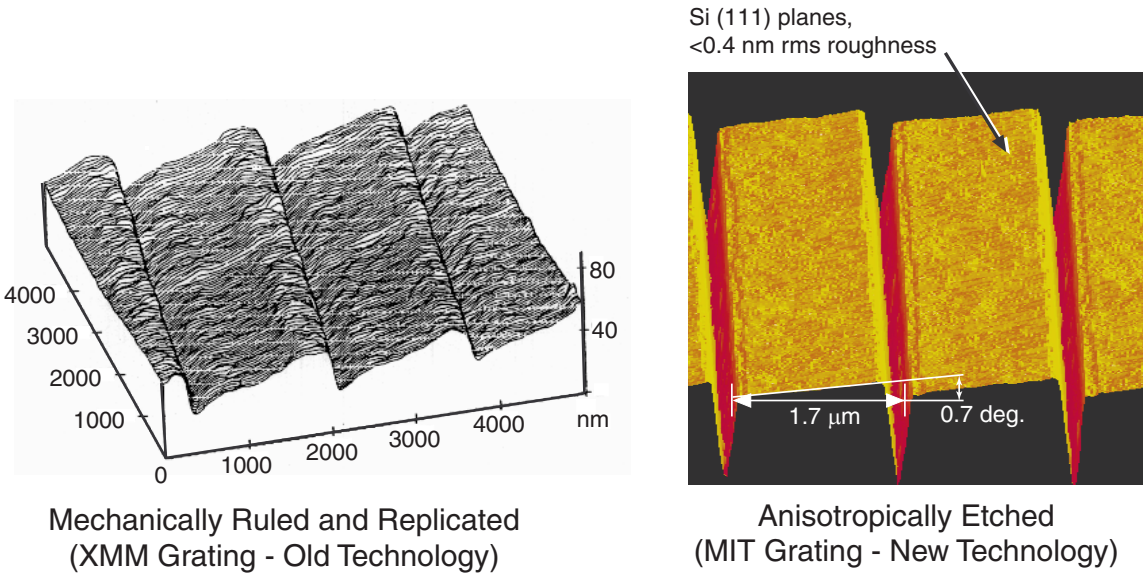

Figure 1. *(a) An AFM image of a traditional mechanically-ruled and replicated x-ray reflection grating (Bixler et al., Proc. SPIE* ***1549****, 420-428 [1991]). Note the rough, wavy groove surface that leads to poor diffraction performance. (b) An AFM image of a blazed x-ray reflection grating fabricated by anisotropic etching of special off-cut (111) silicon wafers. Note the improvement of groove surface flatness and smoothness, leading to significantly improved performance.*

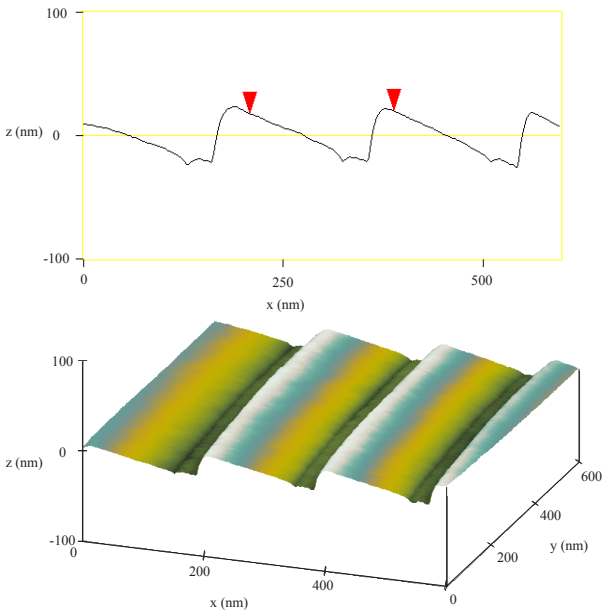

Figure 2*. AFM image of 200 nm-period thermal-nano-imprint grating with 7° blaze angle. The groove surfaces are extremely smooth with a RMS surface roughness of <0.2 nm.*

24. X-ray Foil Optics Shaping Technology

Sponsors:
NASA (NAG5-5405, NAG5-12583), QED, Inc.

Project Staff:
Mirelle Akilian, Craig Forest, Dr. Ralf Heilmann, Y. Sun, Prof. Claude R. Canizares, Dr. George R. Ricker and Dr. Mark L. Schattenburg

Future x-ray astronomy missions will require orders-of-magnitude increase in collecting area and resolution. Thin-foil optics are attractive candidates for x-ray telescopes because of the tremendous weight and cost savings which can be achieved compared to traditional monolithic optics. However, substantial improvement in our ability to shape foils to high accuracy is required. In this research program we are developing technology for high-volume shaping of thin (~0.5 mm) glass and silicon substrates, including both reflective and diffractive components.

Over the last several years we have developed methods for thermally shaping glass sheets. This process involves heating the sheet in a furnace until it begins to slump, conforming to quartz or silicon mandrels that have been lithographically patterned with thousands of pins. The pins reduce the surface area of the mandrel to minimize sticking and mitigate the effects of dust particles. We have also investigated an alternative slumping method based on air bearings.

We are also developing a complementary shaping process called block lapping. This novel process involves the bonding of foils to rigid polishing blocks, while in their relaxed state, using special UV-cured epoxies and thermoplastics. The bonded foils are then mechanically polished into the desired shape.

A third method involved a process called magneto-rheologic fluid polishing (MRF) to deterministically shape the surface of the substrate. A magnetic polishing compound is entrained onto a spinning sphere that is scanned over the substrate. A magnetic field stiffens the fluid in a confined area generating high shear polishing forces. This method requires an accurate surface error map as input to the MRF shaping machine. With this method we were the first group to obtain sub-micron flatness silicon wafers (see Fig. 1).

A critical component of this research is accurate surface metrology of thin foils. We are developed a novel deep-UV Shack-Hartmann surface metrology tool for this purpose (see Fig. 2), and special fixturing that holds the sheets during metrology while minimizing holding torques and gravity distortions (Fig. 3).

Our short-term goal is to develop foil shaping technology with sub-500 nm accuracy. This will enable a number of important NASA missions such as *Constellation X*. Our long term goal is to realize sub-20 nm shaping accuracy, which will enable diffraction-limited x-ray imaging with resolution improved ~1000X more than today's telescopes.

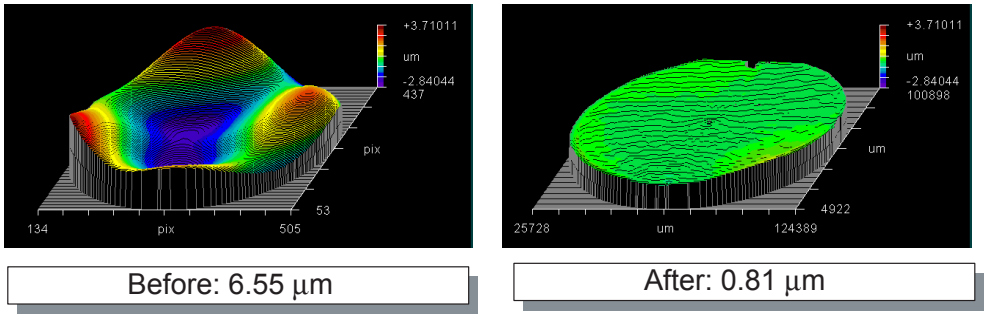

Figure 1. *Interferograms of a silicon wafer before and after magneto-rheologic fluid polishing.*

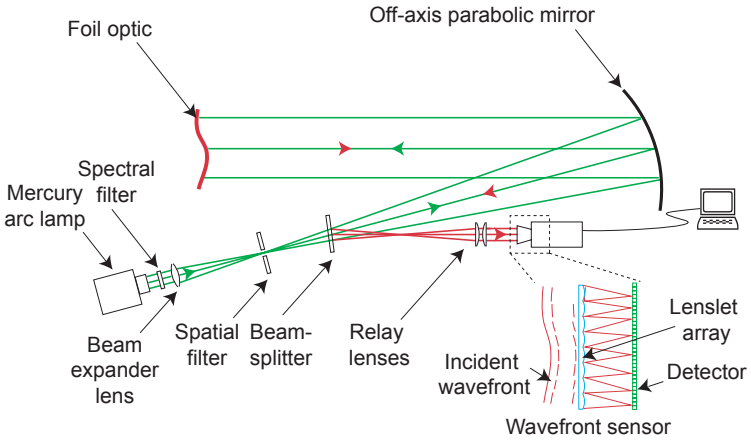

Figure 2. *Schematic of deep-UV Shack-Hartmann topograph metrology tool for the characterization of thin flat substrates.*

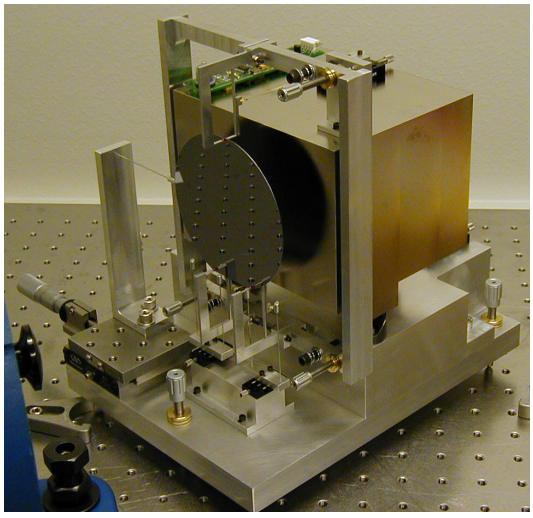

Figure 3. *Photograph of a novel tool for holding thin optics without imparting distortion due to friction, gravity sag or thermal expansion.*

25. Nano-Accurate Assembly Technology for X-ray Foil Optics

Sponsors:
NASA (NAG5-5405, NAG5-12583)

Project Staff:
Mirelle Akilian, Craig Forest, Dr. Ralf Heilmann, A. Torkaman, Prof. Claude R. Canizares, Prof. Alex Slocum, Dr. George R. Ricker and Dr. Mark L. Schattenburg

Future x-ray astronomy missions will require orders of magnitude increases in collecting area and resolution. Foils optics are attractive candidates for x-ray telescopes because of the tremendous weight and cost savings which can be achieved compared to traditional monolithic optics. However, substantial improvements in our ability to assemble foils with high accuracy are required. In this research program we are developing microstructures to assemble foil optics, including both reflective and diffractive components.

Plasma micromachining is used to lithographically fabricate silicon "micro-combs" designed to guide and register silicon and glass foils into precise three-dimensional shapes with sub-micron accuracy. Thousands of ~500 μm-thick foils are typically required in an x-ray telescope, each shaped and assembled to form the precise curves or flats that focus x-rays by grazing-incidence reflection. Fig. 1 shows SEM images of two types of micro-combs under development.

A prototype flight mirror structure based on these principles has been built and tested. Test results show that glass sheets are assembled to a repeatability of ~0.3 micron, corresponding to an angle error of <1 arc-second. This accuracy exceeds previous foil assembly methods by a factor of ~100. Our microstructure technology is being supported by NASA as the baseline technology for assembling foil optics in the *Constellation X* telescope. A photograph of the assembly tooling utilizing the micro-combs is shown in Fig. 2.

Recent effort seeks to improve the accuracy of the micro-combs from the current level of ~200 nm to under 100 nm. With further progress it may be possible to achieve diffraction-limited x-ray imaging, which can potentially improve the accuracy of telescopes by over 1000X.

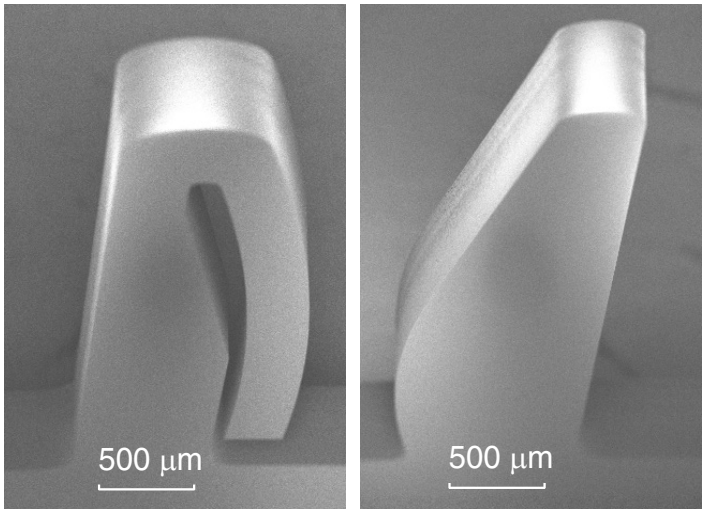

Figure 1. *Electron micrographs of silicon micro-combs. Teeth are ~500 μm wide. a) Spring comb. b) Reference comb.*

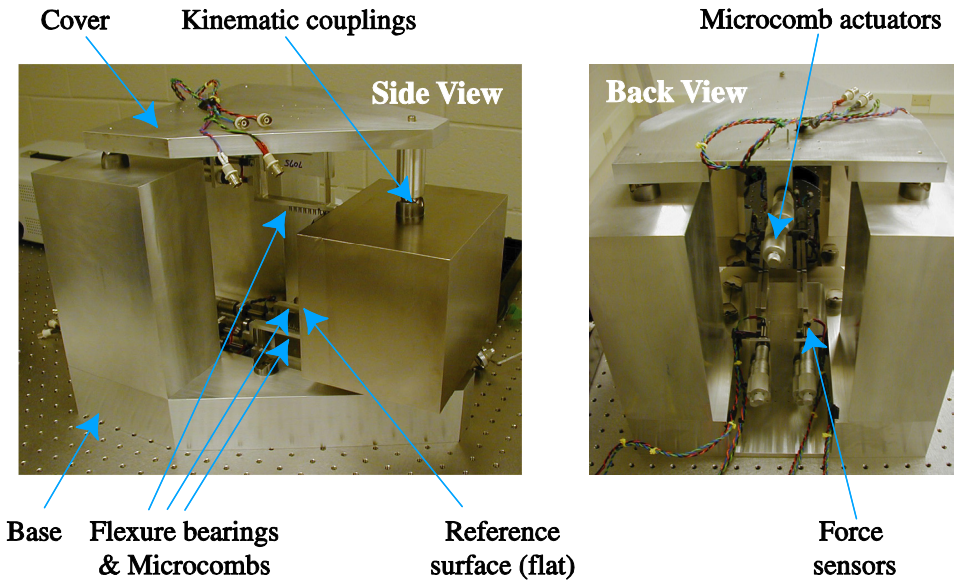

Figure 2. *Photographs of ultra-high accuracy assembly tooling for accurate and repeatable assembly of thin optics utilizing micro-machined silicon structures.*

26. Fabrication of Three Dimensional Nanostructures by Strain Induced Folding: The Nanostructured Origami™ Process

Sponsors:
MARCO (B-12-M06-52)

Project Staff:
Will Arora, Hyun Jin In, Professor Henry I. Smith, Professor George Barbastathis

Nanofabrication technology has developed to the point where, at least in the laboratory, features on the order of 10nm can be patterned and positioned on a substrate with an accuracy of the order of 1nm. However, the fabrication process is still planar, and multilevel structures must be formed layer by layer. Another approach to forming multilevel structures is to fold and stack many layers. Thus, each layer is patterned in one step and then they are all folded in a subsequent step. The goal of this research is to investigate the possibility of such a folding scheme with 180^{o} bends that are caused by mechanical strain and self-actuated by controlled etching.

This method of formation of three-dimensional structures has been observed in the field of biology, where many structures are comprised of folded two-dimensional surfaces. The neural cortex is an example. The circuitry in the brain is laid out over a two dimensional membrane, but folded to allow connections to be made between layers. Currently the number of interconnections needed for a planar microprocessor is given by Rent's rule; however a folded structure with intra- and inter-chip connections would greatly reduce this number and thus extend processor capabilities.

Although several methods of folding thin films have been studied recently, this research focuses solely on strain based folding of thin films. We have chosen silicon nitride as the thin film layer to be folded because of its ease of use and because it can be deposited with very low residual stresses. We have chosen chromium as the material for inducing folding because it can be evaporated with high tensile stress. When released from a silicon substrate, a bilayer thin film consisting of silicon nitride and chrome will curl in order to relieve the strain between the layers. We exploit this curling to fold the silicon nitride 180 degrees and create a layered structure. Initial applications of this folding will be to create stacked diffractive optics. Diffraction gratings, for example, will be patterned on the silicon nitride before the folding step takes place.

We have identified the main challenges associated with folding.

1. Characterization of strain and bending in bi-layer structures
    a. Model of bending as a function of relevant parameters (residual stress, layer dimensions)
2. Alignment of patterned structures on folded layers
    a. Accuracy of fold: position, height, and angle
3. Repeatability of subsequent folds
4. Ability to fold over or under
5. Ability to sequence folds in time
6. Ability to fold accumulated size / mass of many folds

In order for folding to become a useful tool in nanostructure fabrication, all of these challenges must be solved. They all arise from the objective of purposefully interconnecting two-dimensional surfaces by folding into the third dimension. The folded layers must be aligned to within 10nm for interconnections to link successfully. Therefore, careful analysis of strain induced folding is needed, and a process must be developed which is repeatable. Materials that can be deposited with either compressive or tensile residual stress need to be found to allow both types of in-folds.

Finally, a release process must be developed to allow the sequential folding of complicated structures. One idea is to polish the backside of the wafer at an angle and then etch through it anisotropically so that it will release structures on the topside depending on where they are located with respect to the polished backside.

Presently we have modeled the bending of a bilayer structure as follows:

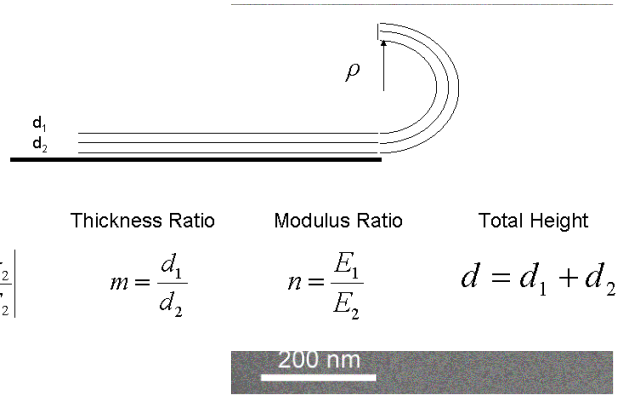

Where the radius of curvature, *p*, is equal to:

$$\rho = \left[\frac{d_2}{6\varepsilon}\right] \cdot \left[\frac{n^2m^4 + 4nm^3 + 6nm^2 + 4nm + 1}{nm(1+m)}\right]$$

Currently we are experimenting to observe the folding effect and confirm this formula for radius of curvature. We are using 200nm of silicon nitride, 100nm of chrome, and expect to see a 20um radius of curvature. The following micrograph shows the bilayer structure from a cross-sectional view:

27. Fabrication of Electrochemical Capacitors via Nanostructured OrigamiTM 3D Assembly and Fabrication Technique

Sponsors:
MARCO (B-12-M06-52)

Project Staff:
Hyun Jin In, Will Arora, Professor George Barbastathis, Professor Henry I. Smith

The Nanostructured Origami™ 3D assembly and fabrication technique has been used previously to successfully demonstrate the folding of 2D membranes patterned with micro and nanoscale features. Lorentz force actuation was used to fold the membranes up to 180 degrees. With several modifications made to the original Nanostructured Origami™ process, an electrochemical capacitor, or supercapacitor, has been successfully fabricated. Unlike a conventional capacitor, an electrochemical capacitor works by forming a double layer capacitance at the interface between the electrolyte solution and a highly porous electrode material. Higher capacitance is achieved due to increased surface area (due to the highly porous electrode surface) and reduced gap distance (limited by the ionic separation distance).

Figure 1 shows the completed device. The finished device consists of two SU-8 membranes connected with gold hinges. Carbon paint is deposited on the top of these membranes to serve as the porous electrode surface, and the membranes are folded so that the two surfaces face each other, effectively forming a capacitor. Although this prototype was folded by hand, future devices will be folded automatically by Lorentz force or residual-stress-induced folding. Devices incorporating the aforementioned folding methods have already been fabricated.

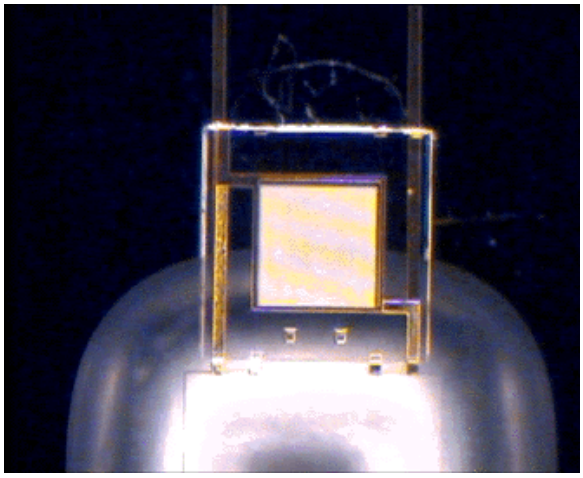

***Figure 1**. Electrochemical capacitor in final, folded form.*

Alignment between the two SU-8 layers has been achieved by forming small pyramids on one of the membranes, and corresponding square openings on the other into which the pyramids will fit. Two pyramids can clearly be seen in Figure 2. With this configuration, alignment better than 2μm has been achieved between the two membranes, and the gap distance between them is also precisely controlled.

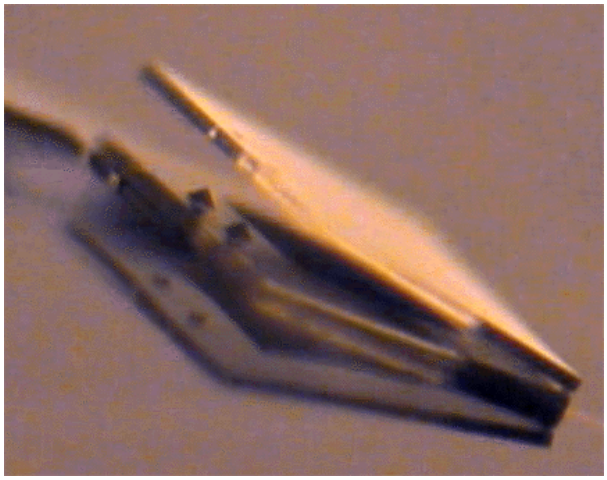

Figure 2. Pyramids for membrane alignment and separation control.

Figure 3 shows the initial popup of the two flaps upon release from the silicon substrate. The highly tensile chromium layer that has been deposited on top of the gold hinge is responsible for this popup as the strain mismatch between the two layers results in a natural bending of the hinge. This phenomenon assists in the folding process, and is being studied as an alternate folding mechanism to the Lorentz force method.

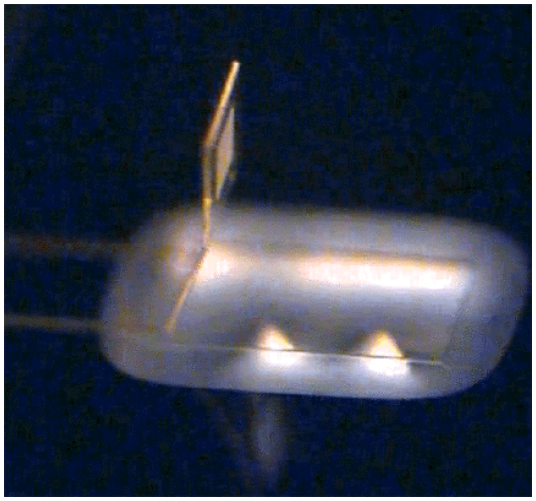

Figure 3. *Initial popup of the SU-8 membranes upon release.*

28. Journal Articles, Published

1. Xiabin Zhu, P. Grutter, Y. Hao, F. J. Castano, S. Haratani, C.A. Ross, B. Vogeli and H.I. Smith, "Magnetization switching in 70 nm-wide pseudo-spin-valve nanoelements", J. Appl. Phys. 93(2), 1132-1136. (2003).

2. John G. Hartley, Timothy R. Groves, Henry I. Smith, Mark K. Mondol, James G. Goodberlet, Mark L. Schattenburg, Juan Ferrera and Alexandr Bernshteyn, "Spatial-phase locking with shaped-beam lithography", Review of Scientific Instruments, Vol. 74(3), 1377-1379, (2003).

3. F. J. Castano, C.A. Ross, C. Frandsen, A. Eilez, D. Gil, Henry I. Smith, M. Redjdal and F.B. Humphrey, "Metastable states in magnetic nanorings", Physical Review B, 67, 184425, (2003).

4. Y. Hao, C. A. Ross, Henry I. Smith, "Thermal stability of lithographicaly patterned sub-200 nm NiFe elements", J. Appl. Phys. 93(10), 7909-7911 (2003).

5. F.J. Castano, Y. Hao, S. Haratani, C. A. Ross, B. Vogeli, Henry I. Smith, C. Sanchez-Hanke, C.C. Kao, X. Zhu, P. Grutter, "Magnetic force microscopy and x-ray scattering study of 70 x 550 nm2 pseudo-spin-valve nanomagnets", J. Appl. Pys. 93(10), 7927-7929, (2003)

6. X. Zhu, P. Grutter, V. Metlushko, Y. Hao, F. J. Castano, C. A. Ross, B. Ilic, H. I. Smith, "Construction of hysteresis loops of single domain elements and coupled permalloy ring arrays by magnetic force microscopy", J. Appl. Phys. 93(10), 8540-8542, (2003).

7. J. Y. Cheng, C.A. Ross, E.L. Thomas, Henry I. Smith, G.J. Vancso, "Templated Self-Assembly of Block Copolymers: Effect of Substrate Topography", Adv. Mater. 2003, 15 No. 19, October 2. 1599-1602. (2003).

8. Euclid E. Moon, Lynn Chen, Patrick N. Everett and Henry I. Smith, "Interferometric-Spatial-Phase Imaging for 6-Axis Mask control", J. Vac. Sci. Technol. B 21(6), 3112-3115 (2003).

9. Dario Gil, Rajesh Menon and Henry I. Smith, "The Case for Diffractive Optics in Maskless Lithography", J. Vac. Sci. Technol. B 21(6), 2810-2814 (2003).

10. Dario Gil, Rajesh Menon and Henry I. Smith, "Fabrication of High-Numerical-Aperture Phase Zone Plates with a Single Lithography Exposure and no Etching", J. Vac. Sci. Technol. B 21(6), 2956-2960 (2003).

11. X. Zhuang, D. Conkerton, A. Lal, M. Feldman, T. O'Reilly and H.I. Smith, "Adaptive Membrane Masks", J. Vac. Sci. Technol. B 21(6), 3082-3085 (2003).

12. Tymon Barwicz, Henry I. Smith, "Evolution of line-edge roughness during fabrication of high-index-contrast microphotonic devices", J. Vac. Sci. Technol. B 21(6), 2892-2896 (2003).

13. J. T. Hastings, Feng Zhang, and Henry I. Smith, "Nanometer-Level Stitching in raster-Scanning E-Beam Lithography Using Spatial-Phase Locking", J. Vac. Sci. Technol. B 21(6), 2650-2656 (2003).

14. JA-A F.J. Castano, C.A. Ross, A. Eilez, D. Gil and Henry I. Smith, "Magnetization reversal in lithographically defined elliptical-ring nanomagnets", Journal of Physics D: Applied Physics, **36**, 2031-2035 (2003).

28.1 Meeting papers, Published:

1. C. G. Chen, P. T. Konkola, R. K. Heilmann, C. Joo and Mark Schattenburg, “Nanometer-accurate Grating Fabrication with Scanning Beam Interference Lithography”, Proc. SPIE 4936, pp. 126-134, (2003).

2. 1. R. Menon, D. Gil, H. I. Smith, "Zone-plate-array lithography: a maskless fast-turn-around system for microoptic device fabrication", Invited Paper at the Photonics West 2003, 25-31 January 2003, San Jose Convention Center, San Jose, CA USA, Published in the Proceedings of Micromachining and Microfabrication, San Jose, CA, January 25-31, 2003. SPIE vol. 4984, pp.10-17, 2003.

3. S. M. Jurga, C. Hidrovo, J. Niemczura, H. I. Smith, and G. Barbastathis, Nanostructured Origami, IEEE Nanotechology 2003, San Francisco, CA, Aug 12-14 (paper TR-4).

4. Minghao Qi, Steven G. Johnson, J. D. Joannopoulos and Henry I. Smith, "Fabrication of three-dimensional photonic crystals with midgap wavelength at 1.55 um", Conference on Lasers and Electro-Optics (CLEO), Baltimore, Maryland, June 1-6, 2003.

28.2 Conference Presentations:

1. J. Todd Hastings, Mark L. Schattenburg, Paul Konkola, Euclid E. Moon and Henry I. Smith, “Nanoaccuracy: an Essential Element of Nanotechnology”, Japan-US Symposium on Tools and Metrology for NanoTechnology, Cornell University, 21-24, January, 2003.

2. Stanley M. Jurga, Carlos H. Hidrovo-Chavez, Johnathan Niemczura, Henry I. Smith and George Barbastathis, “Nanostructured Origami”, IEEE Nanotechnology conference, August 2003 in San Francisco.

3. C.A. Ross, J.Y. Cheng, Henry I. Smith, E.L. Thomas and G. Vancso, “Magnetic Nanostructures made by self-assembled block copolymer lithography”, AVS 2003 Meeting, November 2-7, 2003, Baltimore Convention Center, Baltimore, Maryland.

4. T. Barwicz, H. Haus, Henry I. Smith, "A three-dimensional analysis of scattering losses due to sidewall roughness in integrated optical waveguides", Conference on Lasers and Electro-optics (CLEO), Baltimore MD, June 2003.

5. R. Krishnan, K. Nielsch, Henry I. Smith, C. A. Ross, C. V. Thompson, “Highly ordered, single-domain alumina nanopore arrays and metallic nanowire arrays on silicon for on-chip integration of semiconductor devices”, 2004 Electrochemical Society Conference, Orlando, Florida, October 2003.

6. Y. Shao-Horn, C. Hidrovo, S. M. Jurga, H. I. Smith, and G. Barbastathis, “Origami fabrication of electrochemical device on the micrometer scale”, 204th Meeting of the Electrochemical Society, Orlando, FL, October 2003 (abstract 1279).

7. H. I. Smith, “The role of lithography and metrology in nanophotonics fabrication”, 2003 Optics in Computing, Technical Digest, June 18-20, 2003 Wyndham City Center, Washington, DC.

8. R. Krishnan, K. Nielsch, Henry Smith, C. Ross, C. V. Thompson, “Fabrication of Highly-Ordered Nanopores and Metallic Nanowire Arrays on Silicon for Nanoscale Electronic Device Applications”, 2003 MRS Fall meeting, Boston, Massachusetts, November 2003.

9. Rajesh Menon, Dario Gil, Amil Patel and Henry I. Smith, “Proximity-Effect Correction in Zone-Plate-Array Lithography”, Micro and Nano engineering International Conference, Cambridge, UK, 22-25, September 2003.

10. Dario Gil, Rajesh Menon, Todd Hastings and Henry I. Smith, "The Promise of diffractive Optics in Maskless Lithography", Proceedings of the 28th International Conference on Micro- and Nano-Engineering 2003, Cambridge, UK 22-25 September 2003.

28.3 Thesis:

1. P. Konkola, “Scanning Beam Inferference Lithography”, Ph.D. Thesis, Department of Mechanical Engineering, June 2003.

2. C. G. Chen, “Beam Alignment and Image Metrology for Scanning Beam Interference Lithography – Fabricating Gratings with Nanometer Phase Accuracy”, Ph.D. Thesis, Department of Electrical Engineering and Computer Science, June 2003.

3. M. W. Meinhold, “X-ray Lithographic Alignment and Overlay Applied to Double-Gate MOSFET Fabrication”, Ph.D. Thesis, Department of Electrical Engineering and Computer Science, May 2003.

4. D. Gil, “Maskless Nanolithography and Imaging with Diffractive Optical Arrays”, Ph.D. Thesis, Department of Electrical Engineering and Computer Science, June 2003.

5. J. Cheng, “Fabrication and Characterization of Nanostructures from Sef-assembled Block Copolymers”, Ph.D. Thesis, Department of Materials Science and Engineering, June 2003.

6. T. Hastings, “Nanometer-Precision Electron-Beam Lithography with Applications in Integrated Optics”, Ph.D. Thesis, Department of Electrical Engineering and Computer Science, June 2003.

7. T. Savas, “Achromatic Interference Lithography”, Ph.D. Thesis, Physics Department. September 2003

8. R. Menon, “Diffractive Optics for Maskless Lithography and Imaging”, Ph.D. Thesis, Department of Electrical Engineering and Computer Science, June 2003.

9. S. Smits, “ Photosensitive Dry Etching of Aluminum with applications in Nanolithography”, M. S. Thesis, Leiden University, Leiden, Netherlands. August, 2003